CSIC
Consejo Superior de Investigaciones Científicas

CONFINEMENT OF CHARGE BY PSEUDOMAGNETIC FIELDS IN GRAPHENE

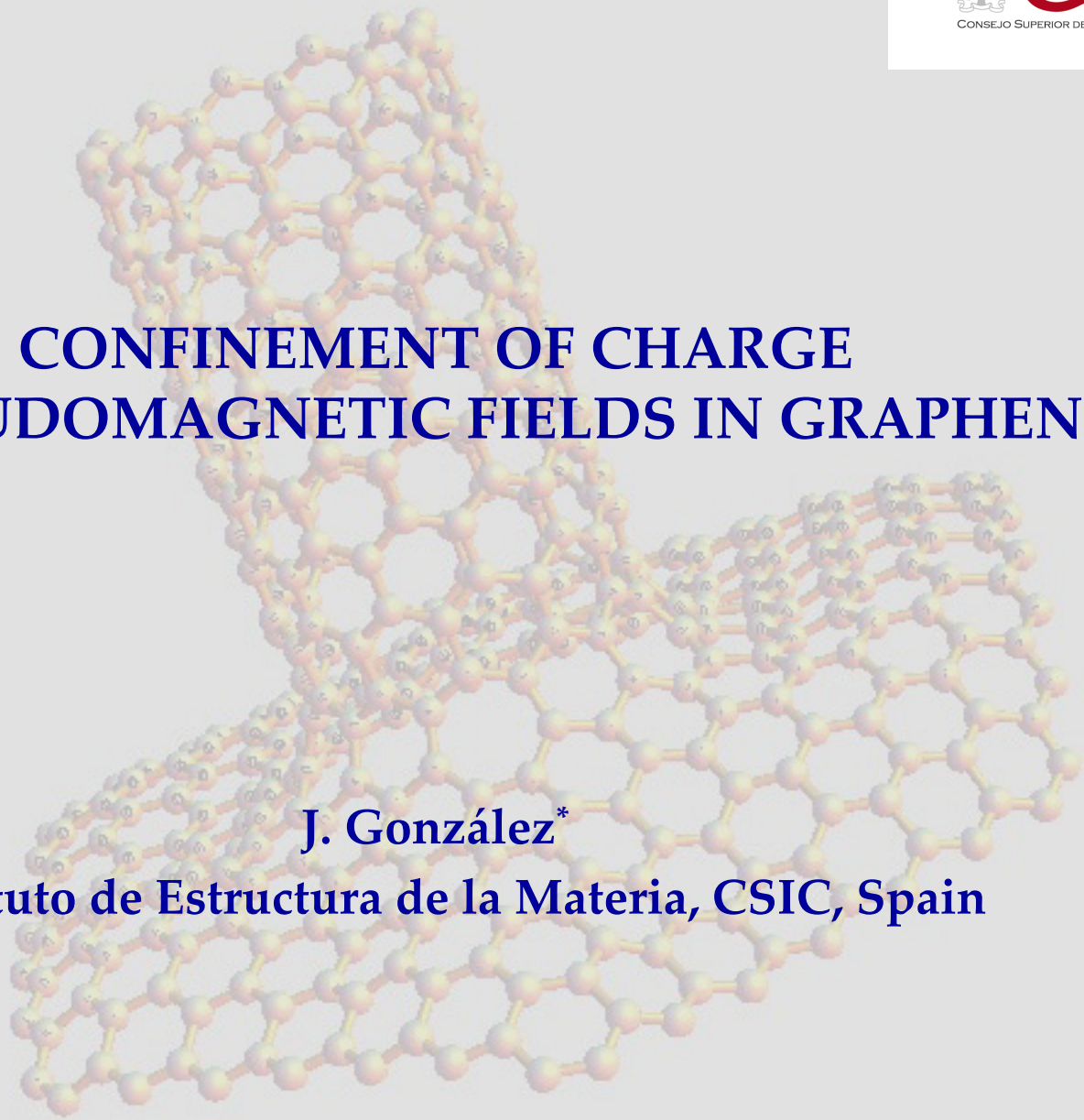

J. González*

Instituto de Estructura de la Materia, CSIC, Spain

*work in collaboration with F. Guinea, J. Herrero and P. San-José

GRAPHENE AS A METALLIC MEMBRANE

Graphene combines in a single material a number of remarkable properties:

- very large speed of charge carriers
- great mechanical strength
- high transparency
- great flexibility

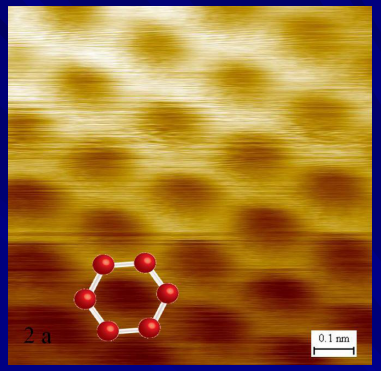

From E. Stolyarova *et al.*, Proc. Natl. Acad. Sci. 104, 9209 (2007)

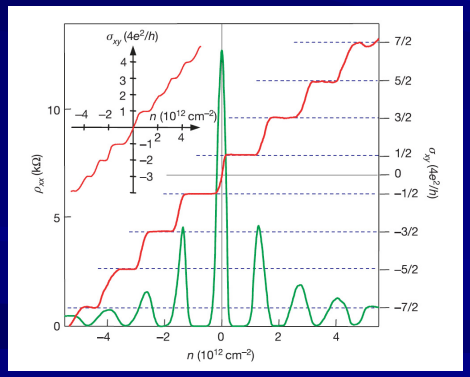

From K. S. Novoselov *et al.*, Nature 438, 197 (2005)
(see also Y. Zhang *et al.*, Nature 438, 201 (2005))

The first clue of new physics was obtained from the observation of the quantum Hall effect:

$$E_N = \mathrm{sgn}(N)\sqrt{2ev_F^2|N|B}$$

ELECTRONIC PROPERTIES OF GRAPHENE

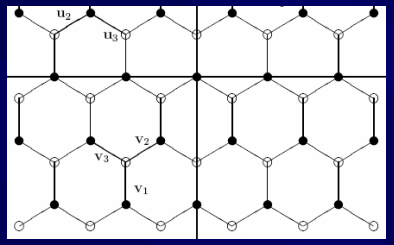

The observed properties were actually consistent with the dispersion expected for electrons in a honeycomb lattice

$$H_{tb} = -t \sum_{r,r'} \psi^{+}(\mathbf{r}')\ \psi(\mathbf{r}) \longrightarrow H = -t \begin{pmatrix} 0 & \sum_a e^{i\mathbf{p}\cdot v_a} \\ \sum_a e^{-i\mathbf{p}\cdot v_a} & 0 \end{pmatrix}$$

$$E = \pm t\sqrt{1 + 4\cos^2(ap_y/2) + 4\cos(ap_y/2)\cos(\sqrt{3}ap_x/2)}$$

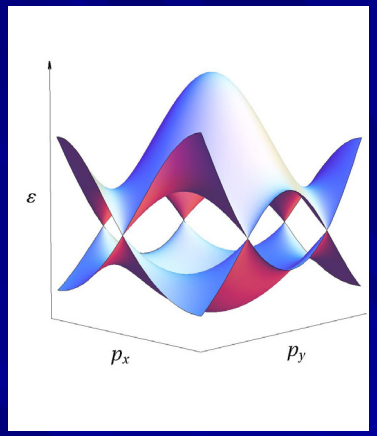

Expanding around each corner of the Brillouin zone, we obtain the hamiltonian for a two-component fermion (Dirac hamiltonian)

$$H = v_F \begin{pmatrix} 0 & p_x - ip_y \\ p_x + ip_y & 0 \end{pmatrix}$$

We have to introduce a Dirac fermion for each independent Fermi point, at which

$$H = v_F \boldsymbol{\sigma} \cdot \mathbf{p} \quad , \quad \varepsilon(\mathbf{p}) = \pm v_F |\mathbf{p}|$$

ELECTRONIC PROPERTIES OF GRAPHENE

The scattering by impurities is quite unconventional in graphene, due to the chirality of electrons. When a quasiparticle encircles a closed path in momentum space, it picks up a Berry phase of π

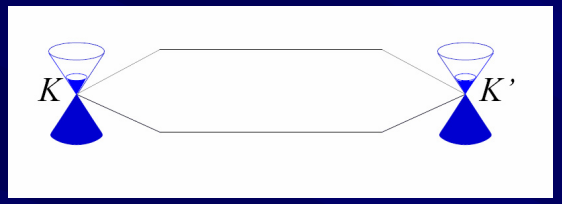

$$H = v_F \begin{pmatrix} 0 & |\mathbf{k}| e^{-i\phi} \\ |\mathbf{k}| e^{i\phi} & 0 \end{pmatrix} \longrightarrow \psi = \frac{1}{\sqrt{2}} \begin{pmatrix} e^{-i\phi/2} \\ \pm e^{i\phi/2} \end{pmatrix}$$

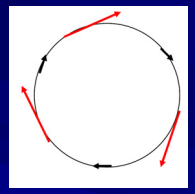

$$\longrightarrow \psi \to e^{i2\pi(\sigma_z/2)} \psi$$

In the absence of scatterers that may induce a large momentum transfer, backscattering is then suppressed (H. Suzuura and T. Ando, Phys. Rev. Lett. 89,266603 (2002)).

$$w \sim |A_{\subset} + A_{\supset}|^2 = |A_{\subset}|^2 + |A_{\supset}|^2 + [A_{\subset}^* A_{\supset} + A_{\subset} A_{\supset}^*] = 0$$

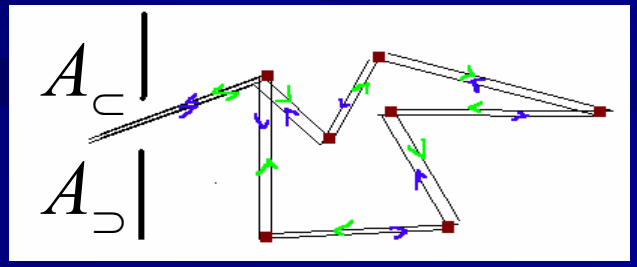

$$A_{\subset} A_{\supset}^* = e^{-i2\pi(\sigma_z/2)} |A_{\subset}|^2 = -|A_{\subset}|^2 < 0$$

ELECTRONIC PROPERTIES OF GRAPHENE

Another way of explaining the suppression of backscattering is by considering that, for the massless Dirac fermions, the pseudospin gives rise to the conserved quantity

$$\boldsymbol{\sigma} \cdot \frac{\mathbf{p}}{|\mathbf{p}|}$$

that changes sign upon the inversion of the momentum.

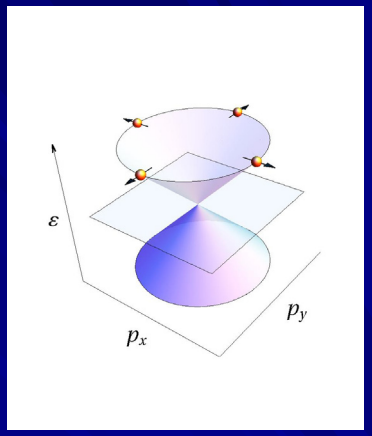

This also explains the peculiar properties of electrons when tunneling across potential barriers: the transmission probability is equal to 1 at normal incidence, and 0 for backscattering

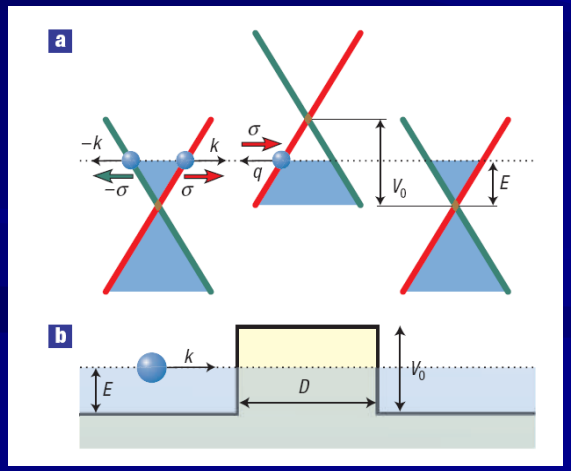

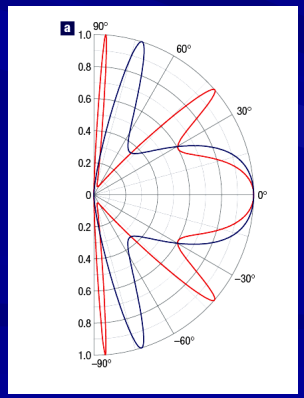

M. I. Katsnelson, K. S. Novoselov, and A. K. Geim, Nature Physics 2, 620 (2006)

GAUGE POTENTIALS IN GRAPHENE

- Gauge potentials from topological defects (pentagonal, heptagonal rings)

  (J. G., F. Guinea and M. A. H. Vozmediano, Nucl. Phys. B 406, 771 (1993))

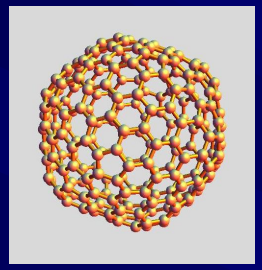

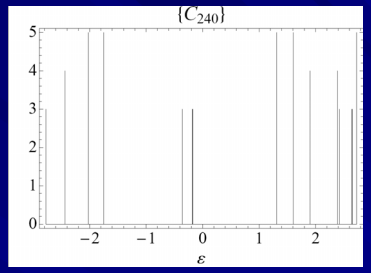

- Gauge potentials from smooth lattice deformations

  (F. Guinea, M. I. Katsnelson and A. K. Geim, Nature Phys. 6, 30 (2009))

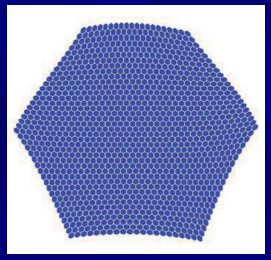

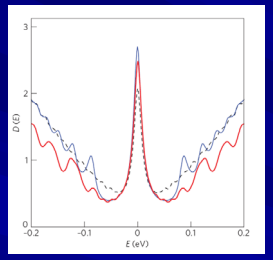

- Gauge potentials from lattice mismatch in graphene bilayers

  (M. Mucha-Kruczynski *et al.*, Phys. Rev. B 84, 041404 (2011); Y.-W. Son *et al.*, Phys. Rev. B 84, 155410 (2011); E. Mariani *et al.*, arXiv:1110.2769) (see also J. Sun *et al.* Phys. Rev. Lett. 105, 156801 (2010))

P. San-José, J. G. and F. Guinea,
Phys. Rev. Lett. 108, 216802 (2012)

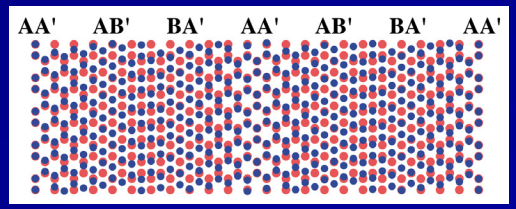

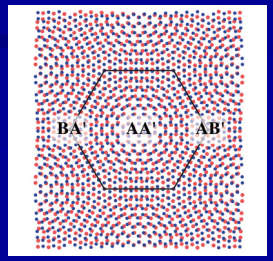

TOPOLOGICAL DEFECTS IN GRAPHENE

The pentagonal carbon rings can be formed by a cut and paste operation in the plane. This induces an effective rotation of $\pi/3$ at the junction, which implies in turn the exchange of the two Dirac valleys

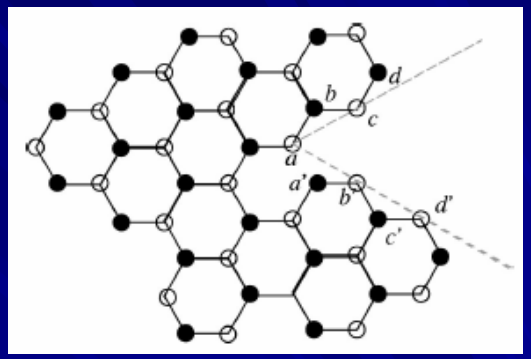

$$\begin{pmatrix} \Psi'_{K} \\ \Psi'_{K'} \end{pmatrix} = \begin{pmatrix} 0 & 1 \\ -1 & 0 \end{pmatrix} \begin{pmatrix} \Psi_{K} \\ \Psi_{K'} \end{pmatrix}$$

The exchange of the two Dirac valleys is only felt when making a complete turn around the topological defect. Therefore, the effect can be mimicked by a line of effective gauge flux Φ threading the pentagonal ring, acting on the (K, K') space

$$A_{\phi} = \frac{\Phi}{2\pi} \begin{pmatrix} 0 & -i \\ i & 0 \end{pmatrix}$$

$$\exp\left(i \oint d\phi \, A_{\phi}\right) = \begin{pmatrix} 0 & 1 \\ -1 & 0 \end{pmatrix} \quad \Leftrightarrow \quad \Phi = \frac{\pi}{2}$$

J. G., F. Guinea and M.A.H. Vozmediano, Nucl. Phys. B 406, 771 (1993)

TOPOLOGICAL DEFECTS IN GRAPHENE

In the fullerenes, the combined effect of the 12 pentagonal rings is consistent with the field of a monopole, whose charge is dictated by the total flux

$$g = \frac{1}{4\pi} \sum_{i=1}^{12} \frac{\pi}{2} = \frac{3}{2}$$

The spectrum is then given in terms of the angular momentum number j

$$\varepsilon_j^2 R^2 = \left(j + \frac{1}{2} \right)^2 - g^2$$

which, for g = 3/2, accounts for the existence of two triplets of zero modes with $j = 1$.

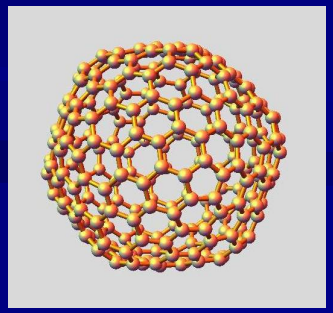

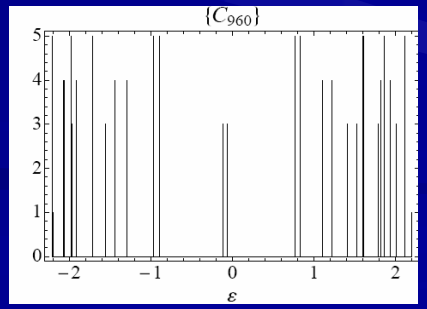

CARBON NANOTUBE-GRAPHENE JUNCTIONS

We can also investigate the effects of negative curvature in graphene. The simplest instance is a carbon nanotube-graphene junction

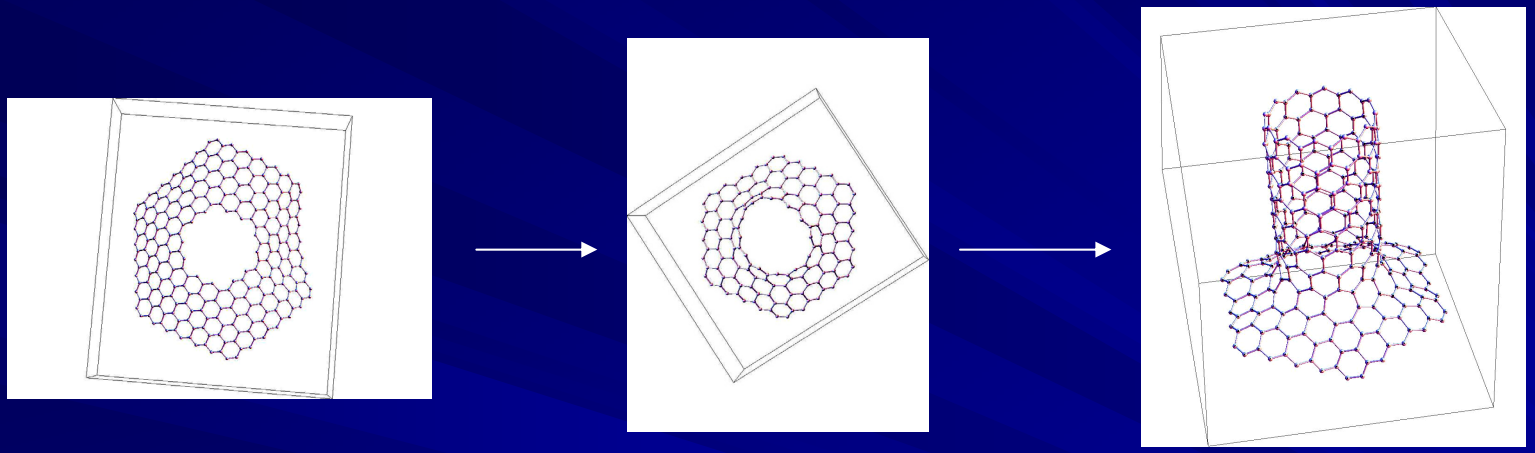

- The nanotube-graphene junction requires an amount of negative curvature corresponding to 6 heptagons

- When the heptagons are regularly distributed, the possible geometries are:
  - zig-zag nanotubes of type ($6n$,0)
  - armchair ($6n$,$6n$) nanotubes

CARBON NANOTUBE-GRAPHENE JUNCTIONS

There is a general, compact way of describing the nanotube-graphene junctions, when the topological defects (heptagons) are regularly distributed. We can think of all possible geometries as assemblies of triangular blocks of honeycomb lattice

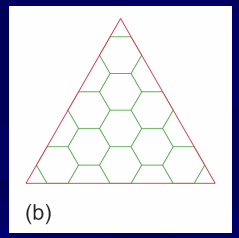

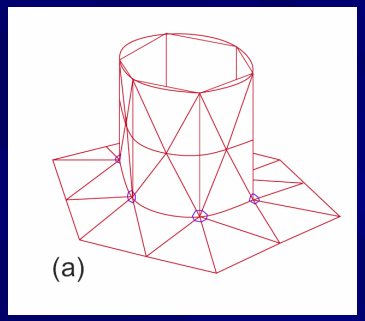

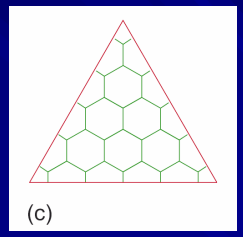

This shows again that the number of heptagonal carbon rings is always the same (6). It also becomes clear that junctions with armchair nanotubes are possible, with geometries $(6n,6n)$.

$(6n,6n)$

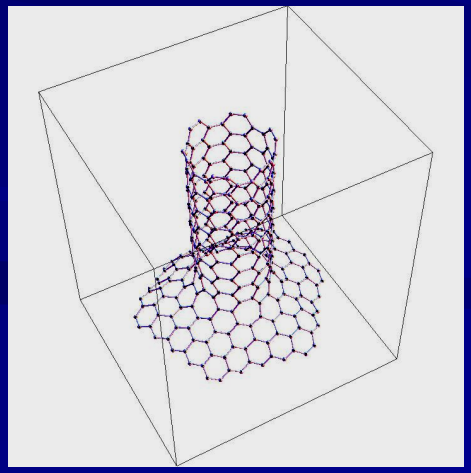

$(6n,0)$

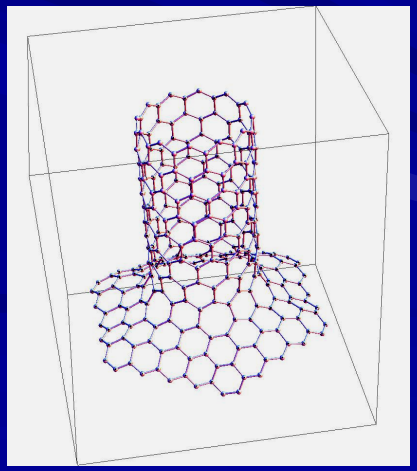

CARBON NANOTUBE-GRAPHENE JUNCTIONS

We may characterize the junctions by looking at the local density of states (DOS) at low energies, in different sectors corresponding to eigenvalue q under a rotation of $\pi/3$:

(a) $q = 1$ (b) $q = e^{\pm i\pi/3}$ (c) $q = e^{\pm 2i\pi/3}$ (d) $q = e^{\pm i\pi}$.

It turns out that all the junctions fall into two different classes, depending on whether the nanotube geometry is $(6n,0)$ with n a multiple of 3 or not.

(18,0)

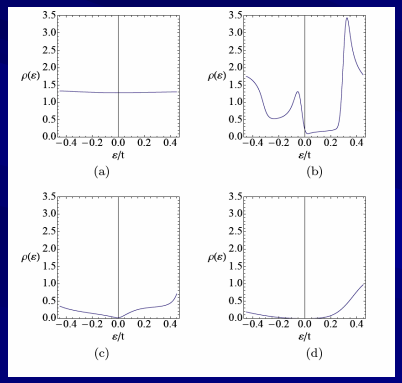

(24,0)

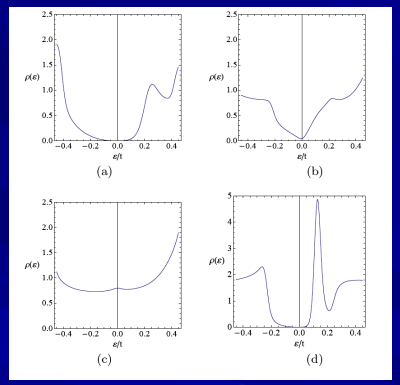

(54,0)

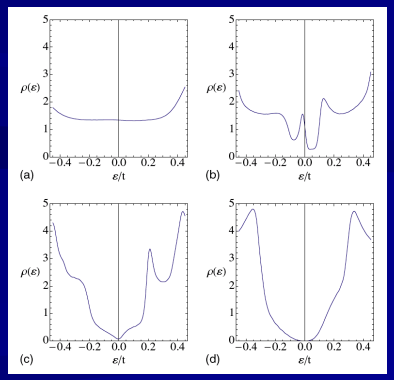

(48,0)

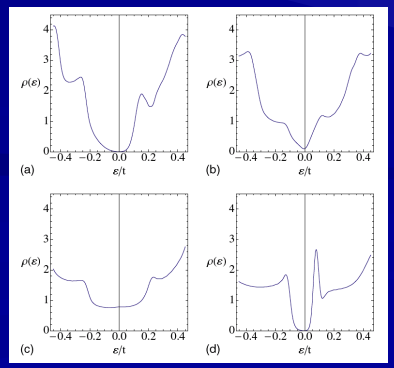

CARBON NANOTUBE-GRAPHENE JUNCTIONS

Within each class, all the DOS look very similar, with the position of the main features scaled in inverse proportion to the radius *R* of the tube:

(12,12)

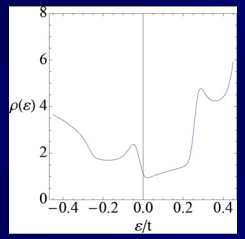

(18,0)

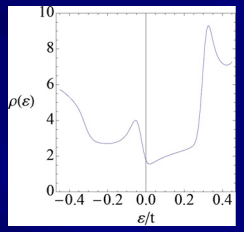

(54,0)

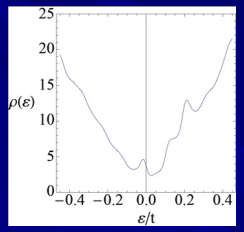

These features can be explained by solving the Dirac equation in the curved space of the junction:

$$iv_F\boldsymbol{\sigma}\cdot\left(\nabla \mp ie\mathbf{A}\right)\Psi^{\pm} = \varepsilon\,\Psi^{\pm}$$

$$\begin{aligned} iv_F\left(\partial_r + \frac{i\partial_\theta}{r} \pm \frac{\Phi}{r} + \frac{1}{2r}\right)\Psi_A^{\pm}(r,\theta) &= \varepsilon\Psi_B^{\pm}(r,\theta) \\ iv_F\left(\partial_r - \frac{i\partial_\theta}{r} \mp \frac{\Phi}{r} + \frac{1}{2r}\right)\Psi_B^{\pm}(r,\theta) &= \varepsilon\Psi_A^{\pm}(r,\theta) \end{aligned}$$

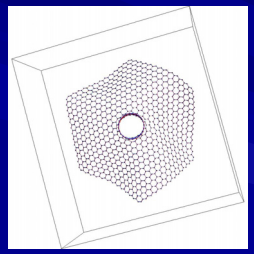

$$\begin{aligned} iv_F\left(\partial_z + \frac{i\partial_\theta}{R_0}\right)\Psi_A^{\pm}(z,\theta) &= \varepsilon\Psi_B^{\pm}(z,\theta) \\ iv_F\left(\partial_z - \frac{i\partial_\theta}{R_0}\right)\Psi_B^{\pm}(z,\theta) &= \varepsilon\Psi_A^{\pm}(z,\theta) \end{aligned}$$

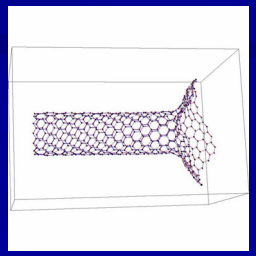

BOUND STATES

What is then responsible for the peaks within the depleted DOS at very low energies?

(12,12)

$q = e^{\pm i\pi/3}$

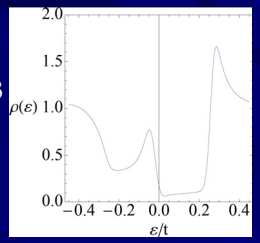

(18,0)

$q = e^{\pm i\pi/3}$

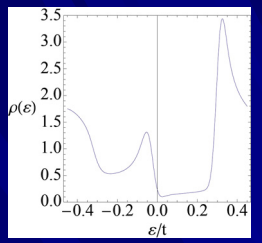

One has to look for bound states of the Dirac equation, that can only take place at $\varepsilon = 0$

$$i\begin{pmatrix} 0 & \partial_r - \frac{1}{r} i\partial_\theta \mp \frac{\Phi}{2\pi r} + \frac{1}{2r} \\ \partial_r + \frac{1}{r} i\partial_\theta \pm \frac{\Phi}{2\pi r} + \frac{1}{2r} & 0 \end{pmatrix} \begin{pmatrix} \Psi_A^{\pm} \\ \Psi_B^{\pm} \end{pmatrix} = 0$$

Taking the maximum flux $\Phi = 3\pi$, it is then possible to have localized states

$$\Psi_A^+ \sim \frac{1}{r^{\Phi/2\pi + 1/2 - m}} e^{im\theta} \quad , \ \Psi_B^+ = 0 \qquad r > R_0$$

$$\Psi_A^+ \sim e^{m(z/R_0)} \, e^{im\theta} \quad , \ \Psi_B^+ = 0 \qquad z < 0$$

We find a state with $m = 1$ which has an amplitude decaying in both the plane and the nanotube, as well as another localized state with $m = -1$ in the other sublattice of the graphene layer.

J. G., F. Guinea and J. Herrero, Phys. Rev. B 79, 165434 (2009)

ARRAYS OF NANOTUBE-GRAPHENE JUNCTIONS

Arrays of carbon nanotube-graphene junctions have been already fabricated in the Fujitsu Laboratories

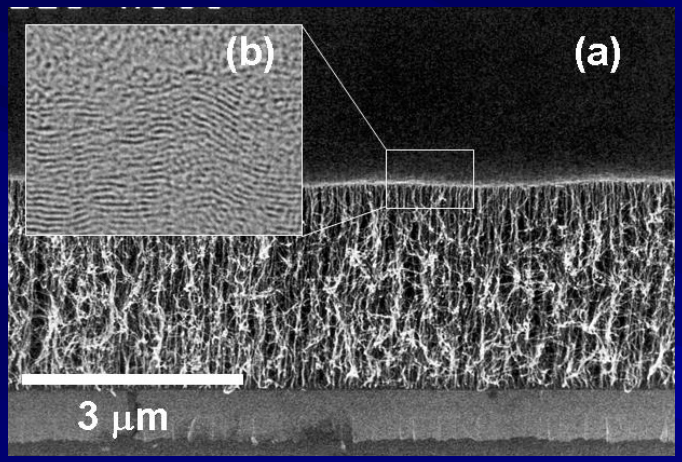

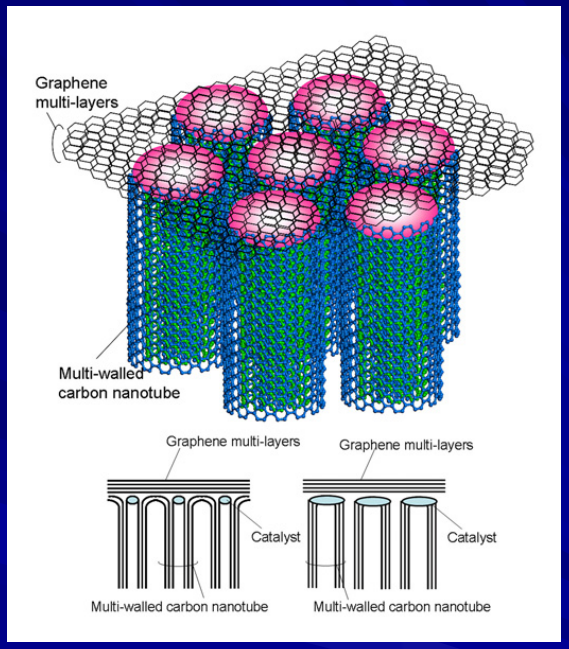

(from Fujitsu Laboratories Ltd.)

ARRAYS OF NANOTUBE-GRAPHENE JUNCTIONS

The arrays of nanotube-graphene junctions have been studied before in the case of very short armchair tubes by T. Matsumoto and S. Saito, J. Phys. Soc. Japan 71, 2765 (2002):

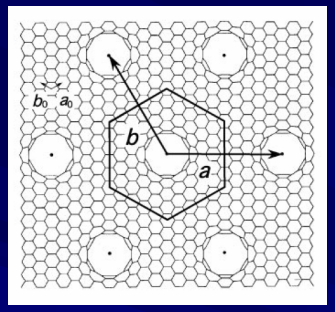

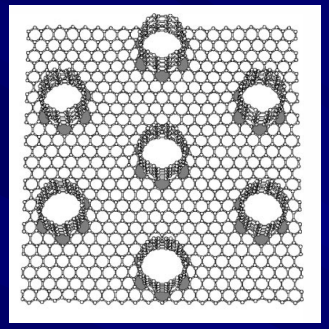

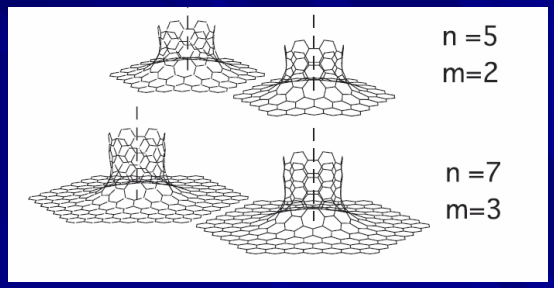

The most important findings were the semiconducting behavior of the undoped system, and the appearance of very flat bands at low energies

C_{162}

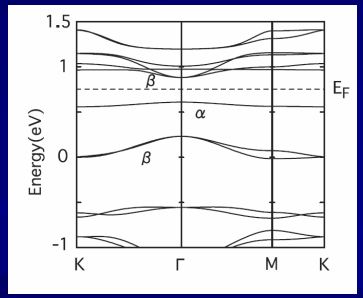

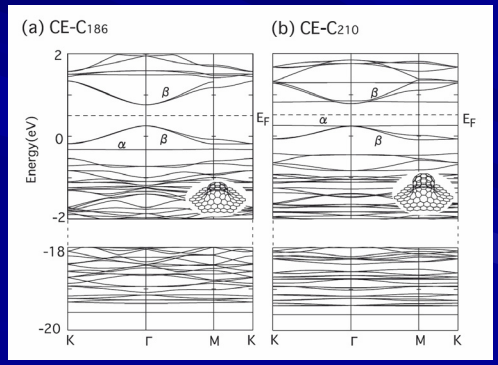

One may ask what would be the electronic structure of junctions with much longer nanotubes, and the dependence on their geometry.

ARRAYS OF NANOTUBE-GRAPHENE JUNCTIONS

We may classify again the different arrays by the geometry of their nanotubes.

One of the classes contains the arrays with armchair or (6*n*,0) nanotubes for which *n* is a multiple of 3. This is characterized by the presence of a series of very flat bands close to the Fermi level:

(12,12)

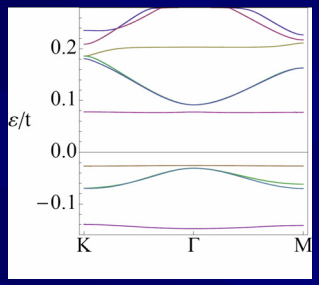

(18,0)

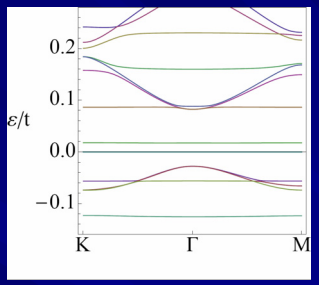

The other class comprises the rest of the arrays, where the bands are in general dispersive:

(12,0)

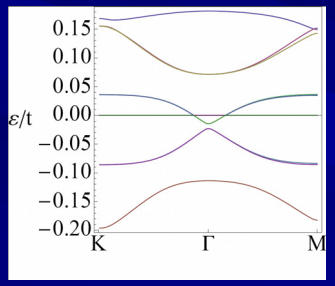

(24,0)

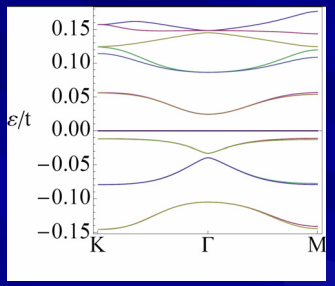

As a general rule:

- the dispersive bands are shifted towards the Fermi level as the distance between the junctions in the array is enlarged
- the number of flat bands grows at low energies as the nanotube length is increased, reflecting that their origin lies in the existence of states confined within the nanotubes

J. G., F. Guinea and J. Herrero, Phys. Rev. B 79, 165434 (2009)

NON-ABELIAN GAUGE FIELDS IN GRAPHENE BILAYERS

It can be shown that graphene bilayers with distinctive Moiré patterns develop confined electronic states according to the structure of the superlattice

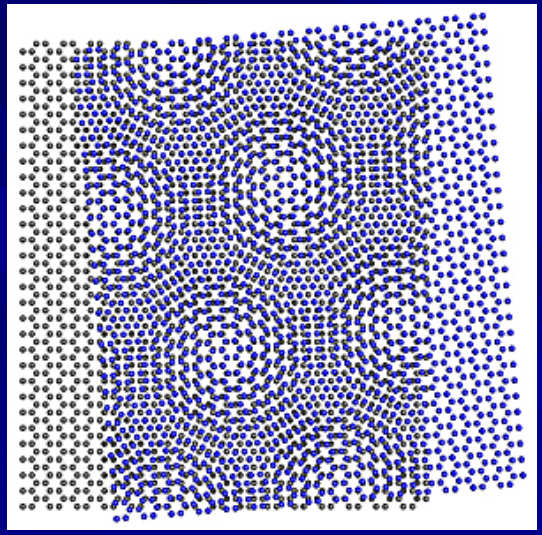

(from National Institute of Standards and Technology)

NON-ABELIAN GAUGE FIELDS IN GRAPHENE BILAYERS

We devise a continuum model for the low-energy electronic states in graphene bilayers

$$H = v_F \begin{pmatrix} 0 & -i(\partial_x - i\partial_y) & V_{AA'}(\mathbf{r}) & V_{AB'}(\mathbf{r}) \\ -i(\partial_x + i\partial_y) & 0 & V_{BA'}(\mathbf{r}) & V_{BB'}(\mathbf{r}) \\ V_{AA'}(\mathbf{r}) & V_{BA'}(\mathbf{r}) & 0 & -i(\partial_x - i\partial_y) \\ V_{AB'}(\mathbf{r}) & V_{BB'}(\mathbf{r}) & -i(\partial_x + i\partial_y) & 0 \end{pmatrix}$$

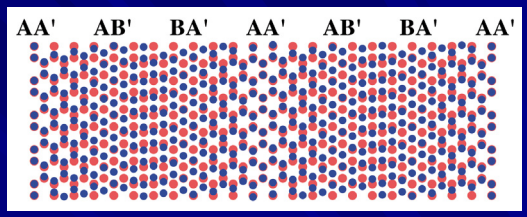

We can decompose the interlayer tunneling amplitudes in the form

$$V_{AB'}(\mathbf{r}) = -A_x(\mathbf{r}) + A_y(\mathbf{r}) \qquad V_{BA'}(\mathbf{r}) = -A_x(\mathbf{r}) - A_y(\mathbf{r})$$

so that A_x and A_y induce an off-diagonal shift of the momenta. We can write in compact form

$$H = v_F \boldsymbol{\sigma} \cdot (-i\partial - \hat{\mathbf{A}}) \;+\; v_F V_{AA'} \tau_1 \qquad \hat{\mathbf{A}} = (A_x \tau_1, A_y \tau_2)$$

The matrix-valued $\hat{\mathbf{A}}$ acts as a genuine gauge potential, giving rise to a Zeeman term

$$v_F^2 \left(-\partial^2 + i\partial \cdot \hat{\mathbf{A}} + 2i\hat{\mathbf{A}} \cdot \partial + A_x^2 + A_y^2 - \sigma_z \hat{F}_{xy} \right) \Psi = \varepsilon^2 \Psi$$

where the pseudospin is coupled to the non-Abelian field strength

$$\hat{F}_{\mu\nu} = \partial_\mu \hat{\mathrm{A}}_\nu - \partial_\nu \hat{\mathrm{A}}_\mu - i\left[\hat{\mathrm{A}}_\mu , \hat{\mathrm{A}}_\nu\right]$$

NON-ABELIAN GAUGE FIELDS IN SHEARED BILAYERS

$$H = v_F \begin{pmatrix} 0 & -i(\partial_x - i\partial_y) & V_{AA'}(\mathbf{r}) & V_{AB'}(\mathbf{r}) \\ -i(\partial_x + i\partial_y) & 0 & V_{BA'}(\mathbf{r}) & V_{BB'}(\mathbf{r}) \\ V_{AA'}(\mathbf{r}) & V_{BA'}(\mathbf{r}) & 0 & -i(\partial_x - i\partial_y) \\ V_{AB'}(\mathbf{r}) & V_{BB'}(\mathbf{r}) & -i(\partial_x + i\partial_y) & 0 \end{pmatrix}$$

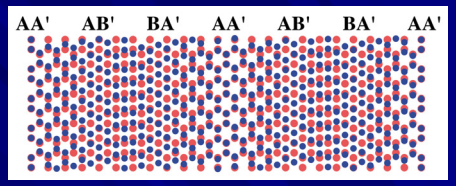

In the case of strained bilayers, the gauge potentials have the periodicity of the Moiré pattern

$$V_{AB'}(x) = -A_x(x) + A_y(x)$$
$$V_{BA'}(x) = -A_x(x) - A_y(x)$$

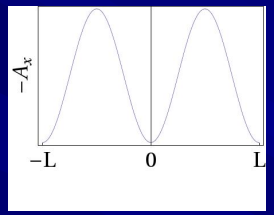

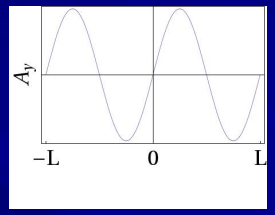

At large period *L*, there is an effective potential that has zeros at the center of *AA′* stacking, and either *AB′* or *BA′* stacking depending on the value of the pseudospin σ_z

$$v_F^2(-\partial^2 + i\partial\cdot\hat{\mathbf{A}} + 2i\hat{\mathbf{A}}\cdot\partial + \underbrace{A_x^2 + A_y^2}$$

$$-\sigma_z(\partial_x A_y \tau_2 - \underbrace{2A_x A_y \tau_3}))\,\Psi = \varepsilon^2\,\Psi$$

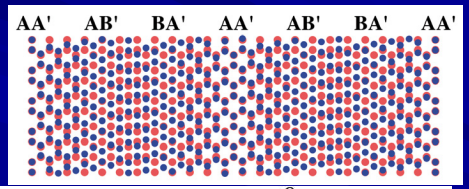

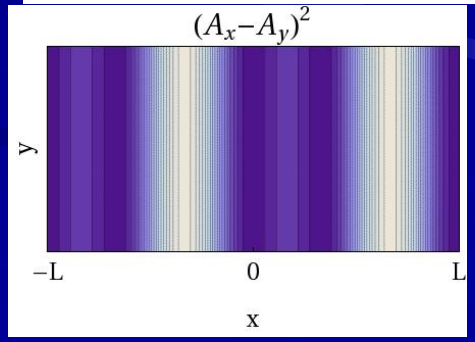

NON-ABELIAN GAUGE FIELDS IN SHEARED BILAYERS

The precise pattern of confinement is found by diagonalizing the full hamiltonian:

$$v_F \left[\sigma_x(-i\partial_x - A_x(x)\,\tau_1) + \sigma_y(k_y - A_y(x)\,\tau_2) + V_{AA'}(x)\,\tau_1\right]\Psi(x) = \varepsilon\,\Psi(x)$$

- For transverse momentum $k_y \neq 0$, the band structure is strongly reminiscent of that found in thick carbon nanotubes in a real perpendicular magnetic field

$k_y \neq 0$ ⟶

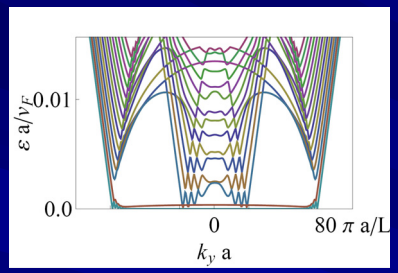

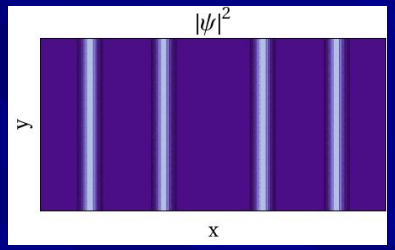

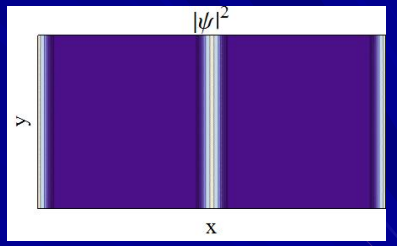

- At transverse momentum $k_y = 0$, we find that the lowest energy subband touches recurrently the level of zero energy, which is a genuine effect of the non-Abelian gauge potential

$k_y = 0$ ⟶

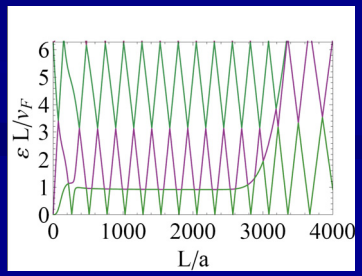

$$\Psi(x)_{\varepsilon=0} = Pe^{i\int_0^x dx'\left[A_x(x')\tau_1 - iA_y(x')\tau_2\right]}\Psi(0)$$

P. San-José, J. G. and F. Guinea,
Phys. Rev. Lett. 108, 216802 (2012)

ELECTRONIC PROPERTIES OF TWISTED BILAYERS

- Low-energy theory in the continuum limit

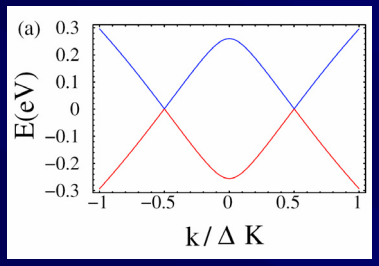

J. M. B. Lopes dos Santos, N. M. R. Peres and A. H. Castro Neto, Phys. Rev. Lett. 99, 256802 (2007)

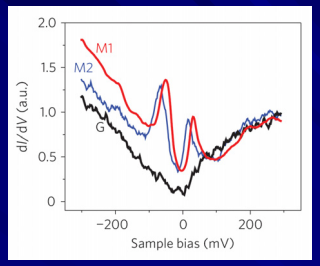

G. Li *et al.*, Nat. Phys. 6, 109 (2010)

- Classification of twisted bilayers

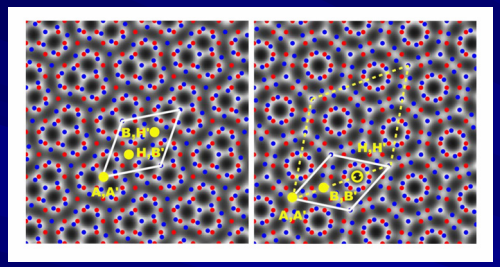

E. J. Mele, Phys. Rev. B 81, 161405(R) (2010)

- Fermi velocity renormalization at small twist angles

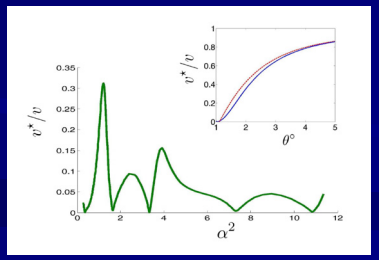

R. Bistritzer and A. H. MacDonald, Proc. Natl. Acad. Sci. 108, 12233 (2011)

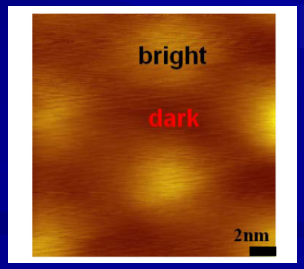

A. Luican *et al.*, Phys. Rev. Lett. 106, 126802 (2011)

R. de Gail *et al.*, Phys. Rev. B 84, 045436 (2011); M. Kindermann and E. J. Mele, Phys. Rev. B 84, 161406(R) (2011); E. Suárez Morell *et al.*, Phys. Rev. B 84, 195421 (2011); E. J. Mele, arXiv:1112.2620; J. M. B. Lopes dos Santos *et al.*, arXiv:1202.1088 .

NON-ABELIAN GAUGE FIELDS IN TWISTED BILAYERS

In the continuum limit (small rotation angles), the low-energy states of twisted bilayers are obtained from the hamiltonian

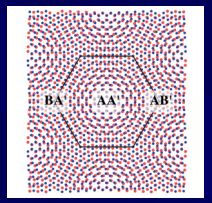

$$H = v_F \begin{pmatrix} 0 & -i(\partial_x - i\partial_y) + i\Delta K/2 & V_{AA'}(\mathbf{r}) & V_{AB'}(\mathbf{r}) \\ -i(\partial_x + i\partial_y) - i\Delta K/2 & 0 & V_{BA'}(\mathbf{r}) & V_{BB'}(\mathbf{r}) \\ V^*_{AA'}(\mathbf{r}) & V^*_{BA'}(\mathbf{r}) & 0 & -i(\partial_x - i\partial_y) - i\Delta K/2 \\ V^*_{AB'}(\mathbf{r}) & V^*_{BB'}(\mathbf{r}) & -i(\partial_x + i\partial_y) + i\Delta K/2 & 0 \end{pmatrix}$$

We define now the gauge fields by

$$V_{AB'} = -A_{1x} + A_{2y} \; + \; i(A_{2x} + A_{1y})$$
$$V_{BA'} = -A_{1x} - A_{2y} \; + \; i(A_{2x} - A_{1y})$$

Introducing the generators $\{\tau_i\}$ of the SU(2) gauge group, we can write in compact form

$$H = v_F \boldsymbol{\sigma} \cdot (-i\partial - \tau_3 \Delta\mathbf{K}/2 \; - \hat{\mathbf{A}}) \; + \; v_F \hat{\Phi} \qquad \hat{\mathbf{A}} = (A_{1x}\tau_1 + A_{2x}\tau_2, A_{1y}\tau_1 + A_{2y}\tau_2)$$
$$\hat{\Phi} = \mathrm{Re}(V_{AA'})\,\tau_1 - \mathrm{Im}(V_{AA'})\,\tau_2$$

We can remove the $\Delta\mathbf{K}$ mismatch of the Dirac cones by means of a gauge transformation

$$\Psi = e^{\frac{i}{2}\tau_3 \Delta\mathbf{K}\cdot\mathbf{r}}\,\tilde{\Psi} \qquad \Rightarrow \qquad H = v_F \boldsymbol{\sigma} \cdot (-i\partial - \hat{\mathbf{A}}) \; + \; v_F \hat{\Phi}$$

NON-ABELIAN GAUGE FIELDS IN TWISTED BILAYERS

An idea of the pattern of confinement in the twisted bilayer can be obtained (at $\Phi = 0$) from

$$v_F^2(-\partial^2 + i\partial\cdot\hat{\mathbf{A}} + 2i\hat{\mathbf{A}}\cdot\partial + \underbrace{A_{1x}^2 + A_{2x}^2 + A_{1y}^2 + A_{2y}^2}$$

$$-\sigma_z(\partial_x A_{1y}\tau_1 + \partial_x A_{2y}\tau_2 - \partial_y A_{1x}\tau_1 - \partial_y A_{2x}\tau_2 + \underbrace{2A_{1x}A_{2y}\tau_3 - 2A_{2x}A_{1y}\tau_3}))\,\Psi = \varepsilon^2\,\Psi$$

The combination $(A_{1x} \pm A_{2y})^2 + (A_{2x} \mp A_{1y})^2$ acts as an effective potential, that keeps the charge density away from the regions of stacking *AB′* or *BA′*

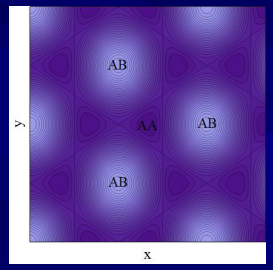

$$(A_{1x} \pm A_{2y})^2$$
$$+ (A_{2x} \mp A_{1y})^2$$

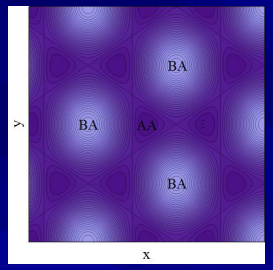

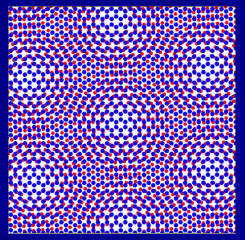

This trend is reinforced by the field strength of $\hat{\mathbf{A}}$, leading to localization around *AA′* stacking

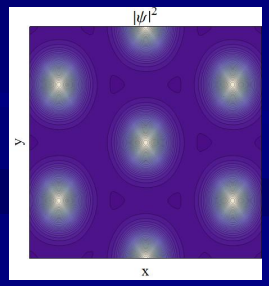

$\theta \approx 1.0°$

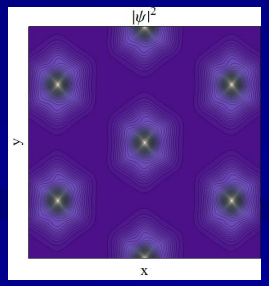

$\theta \approx 0.5°$

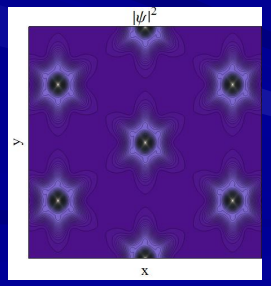

$\theta \approx 0.3°$

(see also G. T. de Laissardière *et al.*, Nano Letters 10, 804 (2010))

NON-ABELIAN GAUGE FIELDS IN TWISTED BILAYERS

Why the magic angles?
The first (largest) angle at which the lowest subband becomes flat corresponds to the situation in which the pseudomagnetic length l_B starts to fit in the unit cell of the superlattice

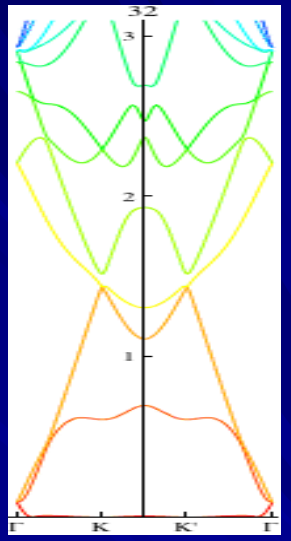

$$l_B \approx \sqrt{\frac{v_F L}{w}} \sim L$$

Actually, the lowest subband becomes flat at the same twist angle that the integral of the field strength over the unit cell equals the quantum of flux ($2\pi\hbar$), up to rotations in SU(2) space:

$$\hat{\phi} = \int_{\text{unit cell}} d^2 r \; \hat{F}_{xy} \approx 2\pi\hbar \begin{pmatrix} 0 & -i\, e^{i2\pi n/3} \\ i\, e^{-i2\pi n/3} & 0 \end{pmatrix}$$

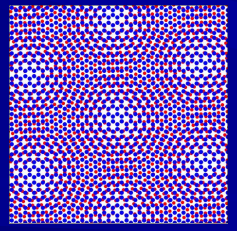

P. San-José, J. G. and F. Guinea, Phys. Rev. Lett. 108, 216802 (2012)

Smaller magic angles are not so simple to characterize, as the scalar potential Φ from the AA' regions starts to have then significant influence on the low-energy subbands.

In conclusion, we have seen that the pseudomagnetic fields that arise in the graphene lattice may provide an efficient mechanism to confine electronic states in the low-lying subbands

- The regular arrangement of the flux from topological defects may lead to bound states in the graphene layer, reflected in the formation of flat bands near the Fermi level

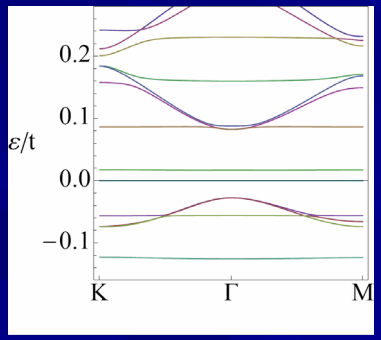

- The mismatch in the registry of graphene bilayers leads to regular patterns of electron localization, with recurrent development of flat bands at zero energy